A spectral model for correcting sun glint and sky glint

P. Gege[1] and P. Groetsch[2, 3]

[1] *Deutsches Zentrum für Luft- und Raumfahrt (DLR), Remote Sensing Technology Institute, Oberpfaffenhofen, 82234 Wessling, Germany. Email: peter.gege@dlr.de*

[2] *Vrije Universiteit Amsterdam, Institute for Environmental Studies (VU-IVM), De Boelelaan 1087, 1081 HV Amsterdam, The Netherlands*

[3] *Water Insight, Marijkeweg 22, 6709 PG Wageningen, The Netherlands. Email: groetsch@waterinsight.nl*

Abstract

Specular reflections of the sun and the sky at the water surface (sun glint, sky glint) can be of comparable intensity or even much higher as the water leaving radiance, even when observation geometry minimizes the sun glint. A number of approaches have been developed for correcting these glint signals, but none of them is working reliably under all conditions. Challenges are the determination of intensity and wavelength dependency of glint in measurements of high spatial and temporal resolution for which the unknown modulations of the water surface by waves are not sufficiently averaged. In general, the reflected radiance differs spectrally significantly from downwelling irradiance, hence their ratio is not a constant, but has a characteristic spectral signature that is mainly determined by scattering processes in the atmosphere. An analytic model has been developed that describes intensity and wavelength dependency of sun glint and sky glint with few parameters. It is implemented in the publicly available software WASI for forward simulation and inverse modeling of radiance and reflectance measurements. Results from applying the model to field measurements are presented.

Introduction

The water surface acts like a mirror and reflects a small part of the sky to a downward looking observer. Reflected radiance originating from the directly transmitted solar irradiance (sun disk) is called sun glint, the reflected diffuse irradiance (sky) is referred to as sky glint. For a plane water surface, the reflected sky area has the size of the observer's field of view, its position follows from the law of reflection, angle of reflection = angle of incidence, and its intensity depends on the angle of incidence as specified by the Fresnel equation. For a wind-roughened or wavy water surface the observed reflections can principally stem from any direction. As glint contributions can be of comparable intensity as the water leaving radiance, or even higher (Figure 1), glint can introduce a noticeable spectral bias to field measurements and remote sensing data, and thus requires an accurate model for correction. A review of methods developed to estimate and remove sun glint from remote sensing imagery is given by Kay et al. (2009), and two recent methods for correcting sky glint from in-situ above-water reflectance measurements were compared by Martinez-Vicente et al. (2013). Both reviews conclude that none of the existing methods works reliably under all conditions.

Model

Spectral radiance upwelling from the water surface, $L_u(\lambda)$, is composed of water leaving radiance, $L_w(\lambda)$, and radiance reflected at the water surface, $L_r(\lambda)$:

$$L_u(\lambda) = L_w(\lambda) + L_r(\lambda). \quad (1)$$

The symbol λ denotes wavelength. The downwelling irradiance at the water surface, $E_d(\lambda)$, is frequently used for normalization since the resulting radiance reflectance depends much less on illumination conditions as radiance itself:

$$\frac{L_u(\lambda)}{E_d(\lambda)} = R_{rs}^{BOA}(\lambda) = R_{rs}(\lambda) + R_{rs}^{surf}(\lambda). \quad (2)$$

Measurements above the water surface allow to obtain $R_{rs}^{BOA}(\lambda)$, called *bottom of atmosphere (BOA) radiance reflectance*. All information about the water body, and eventually the sea floor, is however enclosed in the term *remote sensing reflectance*, $R_{rs}(\lambda)$, which cannot be measured directly. Before this information can be extracted (by means of so-called bio-optical models), the surface radiance reflectance $R_{rs}^{surf}(\lambda)$, or alternatively $L_r(\lambda)$ and $E_d(\lambda)$, must be estimated. Remote sensing additionally requires a reliable estimate for $E_d(\lambda)$ as it cannot be measured at the water surface from airplane or satellite.

Gregg and Carder (1990) have shown for cloudless maritime atmospheres that $E_d(\lambda)$ can be approximated by a sum of three components, representing the "light sources" sun (E_{dd}), blue sky (Rayleigh scattering, E_{dsr}) and aerosols (Mie scattering, E_{dsa}):

$$E_d(\lambda) = E_{dd}(\lambda) + E_{dsr}(\lambda) + E_{dsa}(\lambda). \quad (3)$$

Their model is adopted for the sky radiance (L_{sky}) as follows:

$$L_{sky}(\lambda) = g_{dd} \cdot E_{dd}(\lambda) + g_{dsr} \cdot E_{dsr}(\lambda) + g_{dsa} \cdot E_{dsa}(\lambda). \quad (4)$$

The described glint correction model considers Eq. (4) as a physically reasonable approximation of the radiance reflected at the water surface, where the weights g_{dd}, g_{dsr} and g_{dsa} represent the actual relative contribution of each "light source". The g's are treated as variables that can change from one measurement to the next and may be not known accurately, while the $E(\lambda)$'s are treated as functions with known dependencies on few parameters that can be derived from observations.

A consistent parameterisation of $E_{dd}(\lambda)$, $E_{dsr}(\lambda)$ and $E_{dsa}(\lambda)$ was given by Gregg and Carder (1990). They express them as products of the extraterrestrial solar irradiance, $F_0(\lambda)$, and atmospheric transmittances $T_i(\lambda)$ after scattering or absorption of component i (T_r: Rayleigh scattering, T_{as}: aerosol scattering, T_{aa}: aerosol absorption, T_{oz}: ozone absorption, T_o: oxygen absorption, and T_{wv}: water vapour absorption):

$$E_{dd}(\lambda) = cos\theta_{sun} F_0(\lambda) T_r(\lambda) T_{aa}(\lambda) T_{as}(\lambda) T_{oz}(\lambda) T_o(\lambda) T_{wv}(\lambda). \quad (5)$$

$$E_{dsr}(\lambda) = 0.5\, cos\theta_{sun} F_0(\lambda) (1 - T_r(\lambda)^{0.95}) T_{aa}(\lambda) T_{oz}(\lambda) T_o(\lambda) T_{wv}(\lambda). \quad (6)$$

$$E_{dsa}(\lambda) = cos\theta_{sun} F_0(\lambda) T_r(\lambda)^{1.5} T_{aa}(\lambda) T_{oz}(\lambda) T_o(\lambda) T_{wv}(\lambda)\big(1 - T_{as}(\lambda)\big) F_a. \quad (7)$$

θ_{sun} is the sun zenith angle and F_a the aerosol forward scattering probability. An analytic parameterization of the $T_i(\lambda)$ and F_a was given by Gregg and Carder (1990). The underlying atmospheric database was updated for the range 300-1000 nm in 1 nm resolution by Gege (2012). The water surface reflects a fraction ρ_L of the sky radiance to a downwards looking observer:

$$L_r(\lambda) = \rho_L(\theta_v) \cdot L_{sky}(\lambda). \quad (8)$$

θ_v is the viewing angle. $\rho_L(\theta_v)$ is given for a plane surface and unpolarized light by the Fresnel equation (Jerlov 1976):

$$\rho_L(\theta) = \frac{1}{2}\left|\frac{sin^2(\theta - \theta')}{sin^2(\theta + \theta')} + \frac{tan^2(\theta - \theta')}{tan^2(\theta + \theta')}\right|. \quad (9)$$

θ is the incidence angle as measured from the normal to the reflecting surface, θ' is the angle of refraction. These are related to each other via Snell's law $n_w \sin\theta' = \sin\theta$ with n_w the refractive index of water. The Fresnel reflection factor is ρ_L = 2.0 % for nadir observation and increases for tilted sensors, e.g. to 2.4 % for θ = 40° and 5.9 % for θ= 60°. Combining these equations leads to the following parameterization of $R_{rs}^{surf}(\lambda)$:

$$\begin{aligned} R_{rs}^{surf}(\lambda) &= \frac{L_r(\lambda)}{E_d(\lambda)} \\ &= \rho_L(\theta_v) \cdot \frac{g_{dd} T_r(\lambda) T_{as}(\lambda) + \frac{1}{2} g_{dsr}(1 - T_r(\lambda)^{0.95}) + g_{dsa} T_r(\lambda)^{1.5}\big(1 - T_{as}(\lambda)\big) F_a}{T_r(\lambda) T_{as}(\lambda) + \frac{1}{2}(1 - T_r(\lambda)^{0.95}) + T_r(\lambda)^{1.5}\big(1 - T_{as}(\lambda)\big) F_a}. \end{aligned} \quad (10)$$

Eq. (10) represents a three-component glint model in units of radiance reflectance (sr^{-1}). From the many spectral features of the illumination, introduced by the extraterrestrial solar irradiance and the atmosphere, only Rayleigh and aerosol scattering, $T_r(\lambda)$ and $T_{as}(\lambda)$, remain after normalization to $E_d(\lambda)$. These are spectrally smooth functions without minima or maxima (Gregg and Carder, 1990):

$$T_r(\lambda) = exp\left\{-\frac{M'}{115.6406 \cdot \lambda^4 - 1.335 \cdot \lambda^2}\right\} \ (\lambda \ in \ \mu m), \quad (11)$$

$$T_{as}(\lambda) = exp\{-M \cdot \omega_a \cdot \tau_a(\lambda)\}. \quad (12)$$

M is the atmospheric path length, M' the atmospheric path length corrected for actual air pressure, ω_a aerosol single scattering albedo, and $\tau_a(\lambda)$ aerosol optical thickness. The parameters of ω_a are air mass type, AM, which ranges from 1 (typical of open-ocean aerosols) to 10 (typical of continental aerosols), and relative humidity, RH, with typical values from 46 to 91%. The wavelength dependency of $\tau_a(\lambda)$ approximately follows the Angström law:

$$\tau_a(\lambda) = \beta\left(\frac{\lambda}{\lambda_a}\right)^{-\alpha}. \quad (13)$$

Aerosol optical thickness at λ_a = 550 nm, $\beta = \tau_a(\lambda_a)$, is called aerosol optical depth or turbidity coefficient, and α is known as Angström exponent. β is a standard product of the MODIS satellites (NASA, 2016). Most observations are in the ranges of 0.02-0.2 (mean 0.135) over ocean and 0.02-0.5 (mean 0.21) over land (Remer et al., 2004). β = 0.02 represents a horizontal visibility of 200 km, and β = 0.5 of 7.8 km. α is related to the particle size distribution: the smaller the particles, the larger is α. α ranges approximately from 0.2 to 2.0 (Gregg and Carder, 1990). Typical ranges for our test site, the Baltic Sea, are 0.08-0.22 for β, and 0.7-1.6 for α (Zdun et al., 2011).

Correction algorithm

The correction algorithm provides a method to derive $R_{rs}^{surf}(\lambda)$ from measurement or simulation. The procedure is as follows:

- Step 1: Determine the atmosphere properties $T_r(\lambda)$, $T_{as}(\lambda)$ and F_a.
- Step 2: Determine the reflection factor $\rho_L(\theta_v)$ using Eq. (9).
- Step 3: Determine the glint intensities g_{dd}, g_{dsr} and g_{dsa} by inverse modeling of $R_{rs}^{BOA}(\lambda)$ using Eq. (2).
- Step 4: Calculate the surface reflection $R_{rs}^{surf}(\lambda)$ using Eq. (10).
- Step 5: Subtract $R_{rs}^{surf}(\lambda)$ from $R_{rs}^{BOA}(\lambda)$ to obtain $R_{rs}(\lambda)$.

Step 1. $T_r(\lambda)$ and F_a depend only on air pressure and sun zenith angle and are calculated using equations given in Gregg and Carder (1990). $T_{as}(\lambda)$, however, depends strongly on the not accurately known function $\tau_a(\lambda)$. Its parameters α and β should be determined from measurement to minimize the error of $T_{as}(\lambda)$. α and β can be obtained, for example, from inverse modeling of $L_{sky}(\lambda)$ using Eq. (4), or from inverse modeling of $L_{sky}(\lambda)/E_d(\lambda)$ using Eq. (10) and setting $\rho_L(\theta_v) = 1$ and $g_{dd} = 0$, or from a sun photometer measurement, and from atmosphere correction procedures in case of remote sensing.

Step 3. This step requires a (simple) bio-optical model that can approximate the variability of $R_{rs}(\lambda)$ in the studied area, such as Lee et al. (1998, 1999) or Albert and Mobley (2003). The number of fit parameters should be kept at minimum and their ranges reasonably restricted to keep the risk of fit parameter ambiguity low. If information about optical properties or concentration ranges of the water constituents and eventually the bottom is available, it should be used. Eq. (10) is used to model surface reflections based on $T_r(\lambda)$, $T_{as}(\lambda)$ and F_a from step 1.

Steps 2, 4 and 5 are self-explaining. This procedure is implemented in the "Water Color Simulator" WASI, which is a publicly available software (Gege, 2016) for forward simulation and inverse modeling of radiance and reflectance measurements.

Results

A dataset from the Baltic Sea is used to illustrate how accurate the model can reproduce the spectral variability of glint, how consistent the $R_{rs}(\lambda)$ spectra derived from subsequent measurements are to each other, and how well they correspond to underwater measurements.

Above surface measurements of $L_u(\lambda)$, $L_{sky}(\lambda)$ and $E_d(\lambda)$ were recorded continuously by an Rflex system (Simis and Olsson, 2013) that was installed on the bow of the research vessel M/S Aranda. The system was equipped with inter-calibrated TriOS Ramses-ACC-VIS irradiance and two ARC-VIS radiance sensors (spectral range 320-950 nm), which were mounted on a rotatable platform to maintain an azimuth angle of 90-135° towards the sun if ship orientation allowed. Viewing angles of down- and upwelling radiance sensors were fixed to ~40° from zenith and nadir, respectively, and were not corrected for ship roll or tilt.

771 L_{sky}/E_d measurements were extracted from a dataset collected over ten days of cloudless maritime atmosphere conditions using $L_{sky}/E_d < 0.05$ sr^{-1} at 700 nm. Sun zenith angles ranged from 37° to 62°. The measurements were fitted using Eq. (10) and setting $\rho_L(\theta_v) = 1$ and $g_{dd} = 0$. Figure 2 (left) depicts a representative measurement with a root mean square error (residual) between measurement and fit of 1×10^{-5} sr^{-1}. Typical for blue sky is the strong increase from long to short wavelengths, mainly caused by molecules which scatter the incident sun light out of beam direction with a spectral dependency obeying Rayleigh's law. The scattered photons get lost for the direct beam from the sun, thus the ratio E_{dd}/E_d has a spectral dependency complementary to L_{sky}/E_d (Figure 2, right). As no E_{dd} measurement is available, this plot depicts a simulated spectrum.

Inverse modeling was performed for all L_{sky}/E_d measurements using g_{dsa}, g_{dsr}, α, β as fit parameters. It turned out that g_{dsr} and g_{dsa} are highly correlated at each station. To reduce the number of fit parameters, the average ratio $r_{ar} = g_{dsa}/g_{dsr}$ was determined for each station, and the fits were repeated with just three fit parameters (g_{dsr}, α, β) and setting $g_{dsa} = r_{ar} \cdot g_{dsr}$. This reduction of fit parameters increased the average residual only slightly from 9.11×10^{-5} sr^{-1} to 9.18×10^{-5} sr^{-1}. α has a bimodal distribution with maxima at 0.2 and 1.4, β ranges from ~0 to 0.10 with an average of 0.026 ± 0.013, and the average of g_{dsr} is 0.276 ± 0.026. A comparison of the results for α showed statistical differences for $\beta < 0.006$, but high correlation ($r = 0.96$) above, indicating that reliable estimates of α require $\beta > 0.006$. Spectra $T_r(\lambda)$ and $T_{as}(\lambda)$ typical for these conditions are illustrated in Figure 3.

Once the spectra $T_r(\lambda)$ and $T_{as}(\lambda)$ are known, $R_{rs}^{BOA}(\lambda)$ measurements can be fitted using Eq. (2) to determine the surface reflection $R_{rs}^{surf}(\lambda)$. This was carried out for 118 $R_{rs}^{BOA}(\lambda)$ measurements collected on 12 July 2012 between 9:11 h and 9:50 h UTC at station ID 576 (Figure 1 left). The wind speed of 5.4 m/s roughened the water surface and introduced significant variability to the measurements. Inverse modeling was performed using the software WASI (Gege, 2016) with its implementation of the bio-optical model of Albert (Albert and Mobley, 2003; Albert 2004) for $R_{rs}(\lambda)$ and Eq. (10) for $R_{rs}^{surf}(\lambda)$. The concentrations of chlorophyll-a (C), total suspended matter (X) and absorption of colored dissolved organic matter at 440 nm (Y) were chosen as fit parameters of $R_{rs}(\lambda)$, which is common practice for optically complex deep waters. Since the fits of L_{sky}/E_d had revealed that g_{dsr} and g_{dsa} can be treated together, just two fit parameters were used for $R_{rs}^{surf}(\lambda)$, i.e., g_{dd} and g_{dsr}, while g_{dsa} was calculated as $0.69 \cdot g_{dsr}$ for this station.

Figure 4 (left) illustrates the fit results for a typical $R_{rs}^{BOA}(\lambda)$ measurement from that station. The fit curve (red) matches the measurement (blue) reasonably, but not perfect. Surface radiance reflectance $R_{rs}^{surf}(\lambda)$ (orange curve) was calculated using Eq. (10) with these g_{dsr} and g_{dd}, spectra $T_r(\lambda)$ and $T_{as}(\lambda)$ derived in the previous step, and a Fresnel reflection factor of ρ_L = 2.42 % for

the viewing angle of 40°. Remote sensing reflectance $R_{rs}(\lambda)$ was then obtained by subtracting the calculated spectrum $R_{rs}^{surf}(\lambda)$ from measured $R_{rs}^{BOA}(\lambda)$ (green curve). Note that imperfect matching of the $R_{rs}(\lambda)$ model doesn't affect the result since the $R_{rs}(\lambda)$ model curve is not used for subtracting surface reflections.

This procedure was applied to all 118 measurements at this station. Fit parameter results are C = 2.3 ± 1.3 mg m^{-3}, X = 1.2 ± 0.1 g m^{-3}, Y = 0.45 ± 0.05 m^{-1}, g_{dd} = 0.006 ± 0.002 sr^{-1} and g_{dsr} = 0.52 ± 0.07 sr^{-1}. Figure 4 (right) shows that the derived spectra $R_{rs}(\lambda)$ are consistent with each other (black curves), despite notably variable surface reflections: the relative standard deviations are 36% for g_{dd} and 13% for g_{dsr}. Figure 5 shows that g_{dd} and g_{dsr} are not much correlated. Although g_{dd} is on average almost 100 times lower than g_{dsr} for this dataset, sun glint can have noticeable impact on surface reflections of individual measurements as the sun is much brighter than the sky.

The comparison with remote sensing reflectance spectra derived from underwater measurements (Figure 4 right, green curves) shows good correspondence at short wavelengths, where sky glint introduces a very large bias to $R_{rs}^{BOA}(\lambda)$. The correspondence decreases towards longer wavelengths, but is still reasonable considering the typical uncertainties of underwater measurements and their conversion to above-water reflectance. The underwater measurements are in units of irradiance reflectance and were converted to above surface remote sensing reflectance using Eq. (22) in Lee et al. (1998). The anisotropy factor (ratio of upwelling irradiance to upwelling radiance) in this equation was set to Q = 5. Since it is quite variable and wavelength dependent, but rarely measured, it can introduce significant uncertainty. The effect of changing Q by 10% is indicated by the two curves.

Conclusions

The paper presented a spectral model for simulating sun glint and sky glint and a procedure to correct for these effects in $R_{rs}^{BOA}(\lambda)$ measurements to derive remote sensing reflectance. The model and the correction algorithm, which are implemented in the software WASI, have so far been used to correct for sun glint in airborne (Gege, 2014) and satellite (Dörnhöfer et al., 2016) imagery. Figure 6 shows a result for the multispectral satellite Sentinel-2A. In these applications, only the sun glint parameter g_{dd} was fitted, while sky glint was treated as constant.

The current study applied the method to field measurements which show a strong variability in sky glint due to the small foot print of the radiance sensor and wavy conditions. Sun glint was significantly less intense than sky glint due to the chosen observation geometry (Mobley, 1999), yet still contributed considerably to the variability of $R_{rs}^{BOA}(\lambda)$. The selected example indicates that the model is well suited to describe the spectral properties of $L_{sky}(\lambda)/E_d(\lambda)$, and the correction procedure being able to obtain plausible results for $R_{rs}(\lambda)$. An extended study including an extensive set of field observations and a comparison with other models is in preparation (Grötsch et al., 2017). The correction procedure relies on a suite of parameters, which makes the method susceptible to spectral ambiguities. Thus accuracy of model parameters and choice of fit parameters and ranges can have a strong impact on correction accuracy. A sensitivity analysis related to error propagation is in preparation (Gege and Grötsch, 2017) aiming to optimize the inversion procedure and to estimate error margins.

Acknowlegdement. Reflectance data from the Baltic Sea were collected during cruises SYNTAX10 and SUPREMO12-2 of RV Aranda by the Finnish Environment Institute SYKE, provided courtesy of Stefan Simis. Katja Dörnhöfer is acknowledged for providing the sun glint image of Lake Starnberg.

References

Albert, A., Mobley, C.D., 2003. An analytical model for subsurface irradiance and remote sensing reflectance in deep and shallow case-2 waters. Opt. Express 11, 2873-2890.

Albert, A., 2004. Inversion technique for optical remote sensing in shallow water. Ph.D. Dissertation, Universität Hamburg, Hamburg, Germany, 188pp.

Dörnhöfer, K., Göritz, A., Gege, P., Pflug, B., Oppelt, N., 2016. Water constituents and water depth retrieval from Setinel-2A – a first evaluation in an oligotrophic lake. In review.

Gege, P., 2012. Analytic model for the direct and diffuse components of downwelling spectral irradiance in water. Appl. Opt. 51, 1407-1419.

Gege, P., 2014. A case study at Starnberger See for hyperspectral bathymetry mapping using inverse modeling. Proc. WHISPERS, June 25-27, 2014, Lausanne, Switzerland.

Gege, P., 2016. WASI (Water Colour Simulator). http://www.ioccg.org/data/software.html (accessed 03.10.16).

Gege, P., Grötsch, P., 2017. A four component glint model for correcting water surface reflections. In preparation.

Gregg, W.W., Carder, K.L., 1990. A simple spectral solar irradiance model for cloudless maritime atmospheres. Limnol. Oceanogr. 35, 1657-1675.

Grötsch, P., Gege, P., Simis, G.H., Eleveld, M.A., Peters, S.W.M, 2017. Sun and sky glint correction for remote sensing reflectance observations with a three component glint model. In preparation.

Jerlov, N.G., 1976. Marine Optics, second ed. Elsevier, Amsterdam – Oxford – New York.

Kay, S., Hedley, J. D., Lavender, S., 2009. Sun glint correction of high and low spatial resolution images of aquatic scenes: a review of methods for visible and near-Infrared wavelengths. Remote Sens. 1, 697-730.

Lee, Z.-P., Carder, K.L., Mobley, C.D., Steward, R.G., Patch J.S., 1998. Hyperspectral remote sensing for shallow waters: 1. A semianalytical model. Appl. Opt. 37, 6329-6338.

Lee, Z.-P., Carder, K.L., Mobley, C.D., Steward, R.G., Patch, J.S., 1999. Hyperspectral remote sensing for shallow waters: 2. Deriving bottom depths and water properties by optimization. Appl. Opt. 38, 3831-3843.

Martinez-Vicente, V., Simis, S.G.H., Alegre, R., Land, P.E., Groom, S.B., 2013. Above-water reflectance for the evaluation of adjacency effects in earth observation data: Initial results and methods comparison for near coastal waters in the western channel, UK. Journal of the European Optical Society, 8.

Mobley, C.D., 1999. Estimation of the remote-sensing reflectance from above-surface measurements. Appl. Opt. 38, 7442-7455.

NASA, 2016. Global Maps: Aerosol Optical Depth http://earthobservatory.nasa.gov/GlobalMaps/ Accessed 18 Sept 2016.

Remer, L.A., Tanré, D., Kaufman, Y.J., 2004. Algorithm for remote sensing of tropospheric aerosol from MODIS: Collection 5. In: MODIS ATBD.

Simis, S.G., Olsson, J., 2013. Unattended processing of shipborne hyperspectral reflectance measurements. Remote Sens. Environ. 135, 202–212.

Zdun, A., Rozwadowska, A., Kratzer, S., 2011. Seasonal variability in the optical properties of Baltic aerosols. Oceanologia 53, 7-34.

Figures

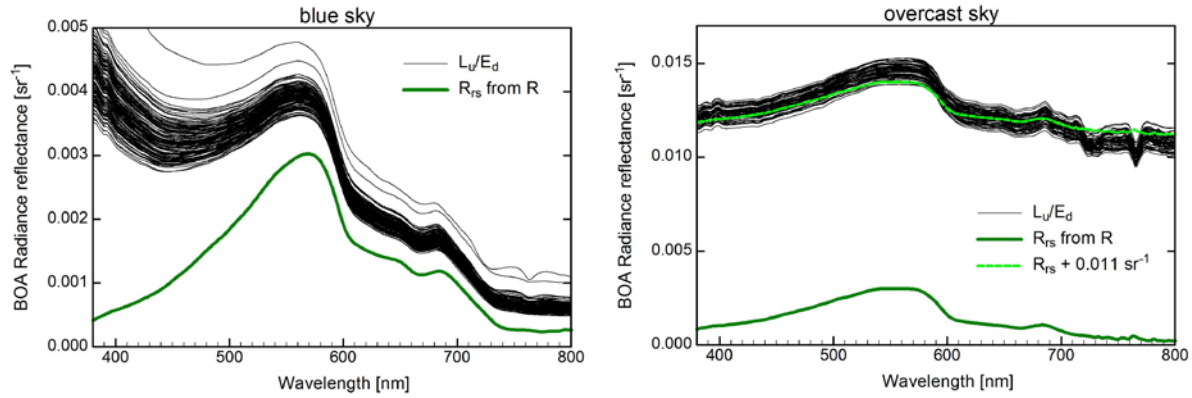

Figure 1. Illustration of the contribution of sky glint to ocean reflectance for blue sky (left) and overcast sky (right). The black curves show measurements above the water surface, the green curves are derived from measurements in water. The difference is due to reflections at the water surface. At blue sky the glint is of comparable intensity as the signal from the water, but shows a strong wavelength dependency. Under overcast sky barely 10% of the measured signal originates from the water; the homogeneous cloud cover introduces a very large offset which is spectrally almost flat (dashed green line).

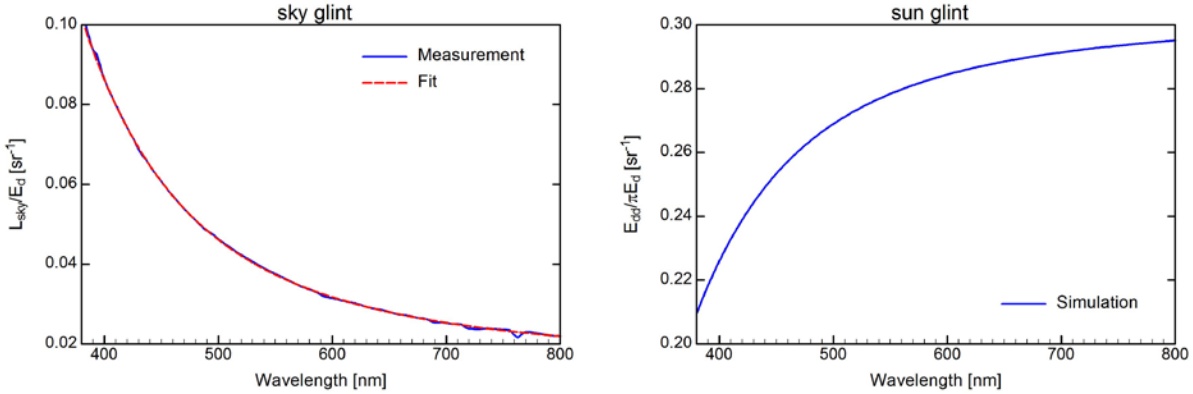

Figure 2. Spectral dependency of sky glint (left) and sun glint (right) in units of radiance reflectance (sr^{-1}) for sun zenith angle = 44°, α = 0.3, β = 0.06. The rms error (residual) of the fit curve (left) is 1.0×10^{-5} sr^{-1}.

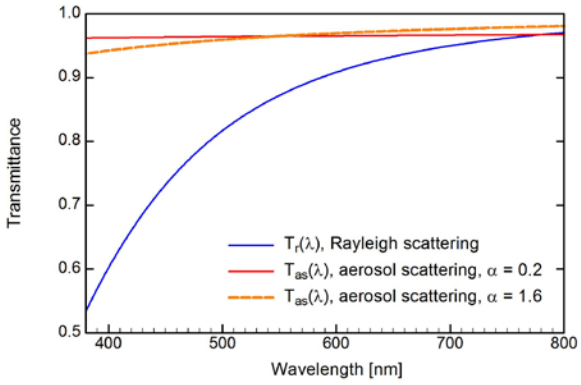

Figure 3. Rayleigh and aerosol transmittance for β = 0.026, sun zenith angle 44.2°, air pressure 1013.25 mbar, AM = 1 and RH = 60%.

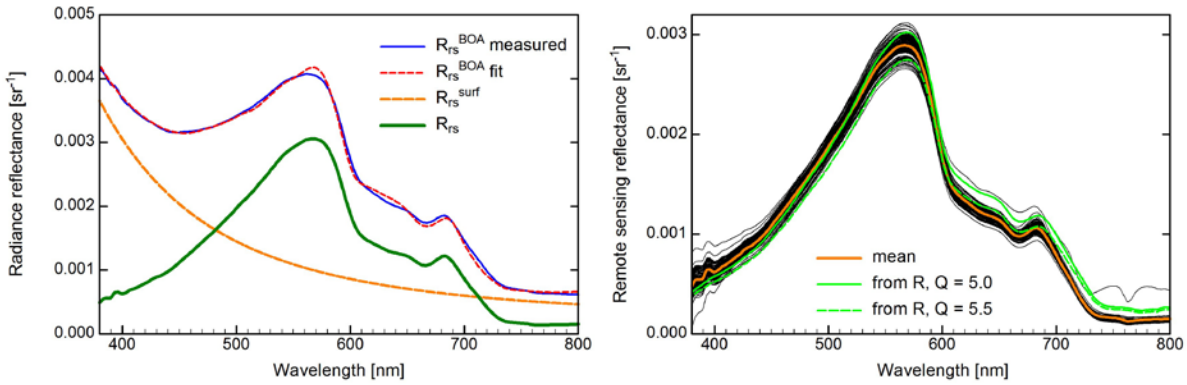

Figure 4. Example for the performance of the correction algorithm. The measurements are from the same station as Figure 1 left.

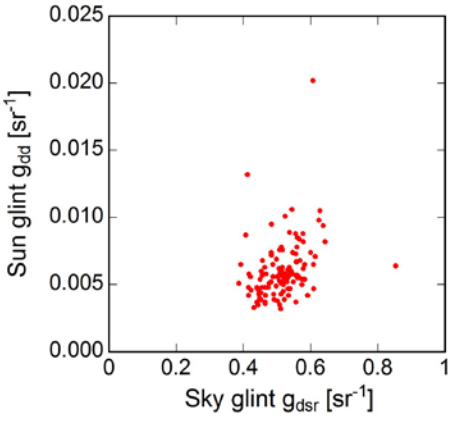

Figure 5. Variability of sun glint (g_{dd}) and sky glint (g_{dsr}).

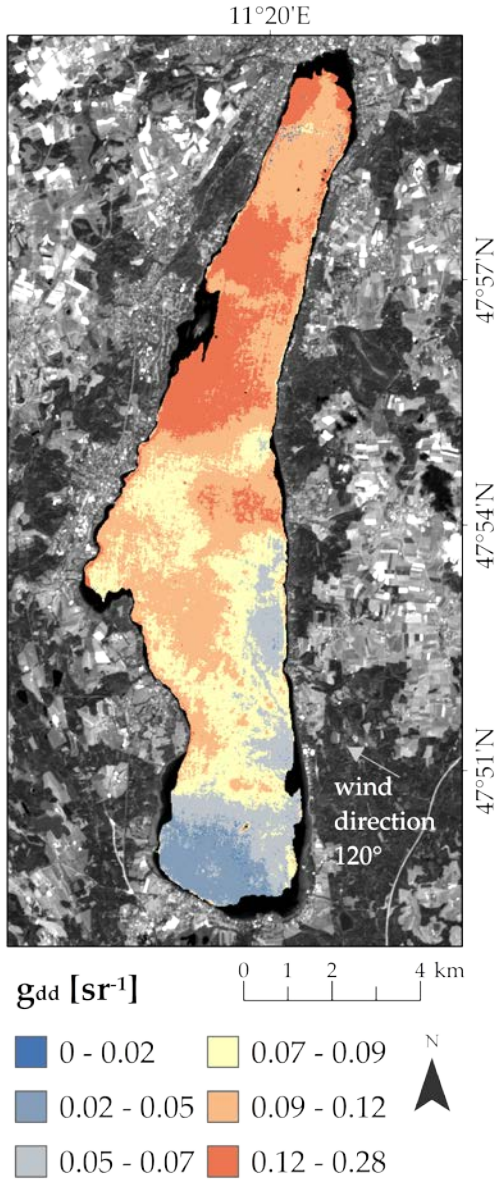

Figure 6: Sun glint image of Lake Starnberg resulting from inverse modeling of Sentinel-2 data using WASI. From Dörnhöfer et al. (2016).